

See discussions, stats, and author profiles for this publication at: <https://www.researchgate.net/publication/251567877>

# Surface Coating of Graphene Quantum Dots Using Mussel-Inspired Polydopamine for Biomedical Optical Imaging

ARTICLE in ACS APPLIED MATERIALS & INTERFACES · JULY 2013

Impact Factor: 6.72 · DOI: 10.1021/am4023863 · Source: PubMed

---

CITATIONS

36

READS

303

## 5 AUTHORS, INCLUDING:



Md. Nurunnabi

Chungnam National University

31 PUBLICATIONS 423 CITATIONS

[SEE PROFILE](#)



Khatun Zehedina

Korea National University of Transportation

13 PUBLICATIONS 315 CITATIONS

[SEE PROFILE](#)



Md Nafiujjaman

Korea National University of Transportation

8 PUBLICATIONS 77 CITATIONS

[SEE PROFILE](#)



Yong-Kyu Lee

Korea National University of Transportation

169 PUBLICATIONS 3,316 CITATIONS

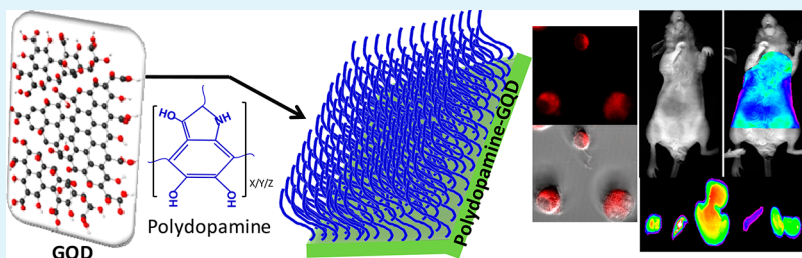
[SEE PROFILE](#)

# Surface Coating of Graphene Quantum Dots Using Mussel-Inspired Polydopamine for Biomedical Optical Imaging

Md Nurunnabi,<sup>†</sup> Zehedina Khatun,<sup>‡</sup> Md Nafiujjaman,<sup>‡</sup> Dong-geun Lee,<sup>§</sup> and Yong-kyu Lee<sup>\*,‡,§</sup>

<sup>†</sup>Department of Polymer Science and Engineering <sup>‡</sup>Department of Green Bio Engineering, <sup>§</sup>Department of Chemical and Biological Engineering, Korea National University of Transportation, Chungju, 380-702 Republic of Korea

 Supporting Information



**ABSTRACT:** Because of the superiority of GQDs (graphene quantum dots) in biomedical imaging, in terms of biocompatibility and toxicity of semiconductor quantum dots, GQDs bring new opportunities for the diagnosis and detection of diseases. In this study, we synthesized photoluminescent (PL) graphene quantum dots (GQDs) through a simple exfoliation and oxidation process, and then coated them with polydopamine (pDA) for enhanced stability in water and low toxicity in vivo. From the results, the GQDs coated with pDA showed an excellent stability of PL intensity. It showed that the PL intensity of noncoated GQDs in PBS solution rapidly decreased with time, resulting in a 45% reduction of the PL intensity for 14 days of incubation in PBS solution. After coating with polydopamine, PL intensities of polydopamine-coated GQDs was maintained more stably for 14 days compared with uncoated GQDs. We have observed the in vitro and in vivo biocompatibility of pDA-coated GQDs in nude mice. The overall observation revealed that pDA-coated GQDs could be used as a long-term optical imaging agent as well as a biocompatible drug carrier.

**KEYWORDS:** *graphene quantum dots, biomedical imaging, polydopamine, photoluminescent*

## 1. INTRODUCTION

In past decades, optical imaging agents based on nanotechnology have been studied extensively to overcome photobleaching and toxicity of organic dyes, to avoid healthy tissue damage by ionization of inorganic optical imaging agents, and to improve the stability of dyes in vivo.<sup>1–7</sup> Compared with organic dyes, inorganic semiconductor quantum dots (QDs) are considered to be one of the most effective materials, showing photobleaching resistant properties and a high quantum yield.<sup>8–14</sup> However, issues of toxicity are prominent among semiconductor QDs, and limited their application in biological system.<sup>15–20</sup> Therefore, several strategies, such as surface modification and polymeric coating have been proposed to minimize the toxicity of semiconductor QDs.<sup>21–26</sup> However, little progress of the toxicity problem is being reported.

Recently, similar applications of carbon-based graphene quantum dots (GQDs) have been reported by a few research groups,<sup>27–30</sup> and their luminescent properties make them a very promising candidate for cell imaging with a visible excitation wavelength.<sup>31–33</sup> Peng et al. reported on the synthesis of blue and green color GQDs from carbon fiber, and also provided adequate evidence to prove the chemical composition of the GQDs, showing that a hexagonal GQDs contains numerous amounts of carboxylic acid and hydroxyl groups, with a specific

energy band gap.<sup>34</sup> They also have demonstrated that excitation-based color is tuned by varying the reaction temperature. Recently, our group reported a simple method to synthesize photoluminescent near-infrared graphene nanoparticles, showing single or multiple graphene layers with a size of only several nanometers.<sup>35</sup>

There are several well-known and well-studied materials such as polyethylene glycol (PEG), PLGA, chitosan, heparin, poly acrylic acid (PAA) introduced for surface coating and functionalize. However in this study we have considered dopamine to functionalize the 2D GQDs surfaces. The 3,4-dihydroxyphenylalanine (DOPA) plays a key role in mussel adhesion in an aqueous environment.<sup>36</sup> It has been widely reported/acknowledged that DOPA is a novel and dramatic material which can be used to modify any smooth or rough surface to make it cohesive and functionalized.<sup>37–40</sup> Hong et al. has reported that pDA-coated QDs greatly reduced the inflammatory response and the immunological responses of blood.<sup>41</sup> In this study, pDA was chosen as a coating material as it has been widely studied to coat graphene, graphene oxide,

**Received:** June 20, 2013

**Accepted:** July 23, 2013

**Published:** July 23, 2013



silver nanoparticle and gold nanoparticles, observed as an emerging bioinspired materials.<sup>42,43</sup>

In this study, mussel-inspired pDA was introduced into the GQDs to interconnect with each other. It is also expected to improve the PL stability of GQDs for a long-term *in vivo*. The particle size of pDA-coated GQDs increased from 9 to 30 nm in diameter, depending on the polymerization duration. The presence of pDA was confirmed on the surface of GQDs by FT-IR and FT-NMR spectroscopic analysis. Thermal stabilities of GQDs and pDA-coated GQDs were compared by TGA and DTA. Most importantly we have investigated the optical imaging profile of GQDs and pDA-coated GQDs in both *in vitro* and *in vivo* systems. The intravenously injected pDA-coated GQDs shows the interesting biodistribution profile in nude mice as observed by noninvasive molecular imaging system. *In vitro* and *in vivo* observations demonstrated that pDA-coated GQDs had improved biocompatibility, and PL stability of GQDs for a long-term. GQDs are considered as a new potential optical imaging agent for *in vitro* and *in vivo* applications, and pDA coating can enhance PL stability in aqueous solution as well as biocompatibility. The pDA-mediated surface-unctionalized GQDs could be further studied to learn feasibility for drug delivery and biomedical imaging.

## 2. EXPERIMENTAL SECTION

**Materials.** Pitch carbon fiber (5–10  $\mu\text{m}$  in diameter) was purchased from Fiber Glast Development Corporation (Carr Drive Brookville, OH). Sulfuric acid, nitric acid, sodium hydroxide, sodium carbonate and dopamine were purchased from Sigma-Aldrich (St. Louis, MO). Cell culture reagents, including fetal bovine serum (FBS), Dulbecco's Modified Eagle Medium (DMEM), penicillin-streptomycin, trypsin/EDTA, and Dulbecco's phosphate buffer saline (PBS) were purchased from Gibco BRL (Carlsbad, CA, USA). 3-(4,5-dimethylthiazol-2-yl)-2 and 5-diphenyl tetrazolium bromide (MTT) were obtained from Amresco Inc. (Solon, OH, USA).

**Synthesis of Photoluminescent Graphene Quantum Dots.** Sulfuric acid (40 mL) and carbon fiber (CF, 100 g) were added to a beaker and were sonicated by ultrasonicator for 10 min at room temperature. Nitric acid (20 mL) and sulfuric acid (40 mL) were added to a three neck flask and were placed in a heating mantle.<sup>35,44</sup> The temperature was adjusted to  $95 \pm 5^\circ\text{C}$  and the previously sonicated carbon fiber solution was slowly injected to the flask by a syringe injector. Reaction was carried out for 12 h at the same temperature. Citric acid (100 mg) was added and stirring was continued for 1 h at  $60 \pm 5^\circ\text{C}$ . An excess amount of water (300 mL) was added slowly to the beaker. Sodium hydroxide and sodium carbonate were added respectively to the solution to bring the pH to 8.0. The flask was placed in an ice bath and the temperature was controlled to  $0\text{--}4^\circ\text{C}$  with slow stirring. Precipitated material was removed from the flask by decantation, and the GQDs containing solution was freeze-dried for 48 h.

**Polydopamine-Coated Graphene Quantum Dots.** The required amount of Tris-buffered saline (TBS, pH typical of marine environments, 2 mg/mL of 10 mM tris, pH 8.5) was added to a beaker.<sup>45</sup> DOPA (30 mg) was dissolved in the buffer and was stirred for 3, 6, and 12 h at room temperature. Hydrochloric acid (0.1 N) was added slowly to the solution until the pH reached 4.5. Degree of polymerization of polydopamines was estimated from the  $^1\text{H}$  NMR spectrum of respective pDA formulations (3, 6, and 12 h). The previously prepared dried GQDs were added to the solution and stirring was continued for 2 h under the same conditions. The solution was dialyzed (MWCO-2000) against water for 12 h to remove the uncoated GQDs and free DOPA. The solution was dried in freeze-dryer for 48 h to result in a dried powder.

**Characterization of GQDs and Polydopamine-Coated GQDs.** The size distribution and morphologies of GQDs nanoparticles were examined using dynamic light scattering (DLS) (ELS-Z2, Otsuka

Electronics Co., Ltd., Japan) and a TEM (JEOL, Japan). Photoluminescence, excitation and emission were measured by luminescent analyzer FluoroMate FS-2 (Scinco, Korea). The thermal stability was studied using a TA-Q50 thermo-gravimetric analyzer (TGA) (TA, state). Each sample (GQDs and pDA-coated GQDs) was heated from room temperature to 500 °C with heating rate of 10 °C/min under a nitrogen atmosphere. The XRD data were collected on a Rigaku D/Max Ultima II Powder X-ray diffractometer (Rigaku Corporation, Japan). XPS analyses were carried out on a PHI Quantera X-ray photoelectron spectrometer with a chamber pressure of  $5 \times 10^{-9}$  Torr and an Al cathode as the X-ray source. The source power was set at 100 W, and pass energies of 140.00 eV for survey scans and 26.00 eV for high-resolution scans were used.

**In Vitro Stability of Polydopamine-Coated GQDs.** To investigate the stability of GQDs nanoparticles, we measured the changes in the fluorescent intensity of GQDs and pDA-coated GQDs nanoparticles in an aqueous solution (PBS), serum solution (10% FBS, 90% PBS) and electrolyte solution (2% NaCl) over time.<sup>46</sup> PL intensity was also observed at four different pH values (5, 7, 9 and 11). GQDs (1 mg/mL) and pDA-coated GQDs nanoparticles (1 mg/mL) were dispersed in different solvents, and changes of PL intensity were monitored for 14 days.

**Cytotoxicity and Cellular Imaging of Polydopamine-Coated GQDs.** *In vitro* toxicity of GQDs and D-GQDs has been examined in KB cells for 24 and 48 h. At  $37^\circ\text{C}$  and a 5%  $\text{CO}_2$  containing humidified atmosphere, cells were grown in a medium containing MEM with 10% fetal calf serum. The cells ( $5 \times 10^4$  cells/mL), grown as a monolayer were harvested by 0.25% trypsin-0.03% EDTA solution. 200  $\mu\text{L}$  KB cells containing medium were placed in 96 well plates and were incubated for 24 h. After 24 h, the complete medium was suctioned and samples were added to the wells at different concentrations (10, 25, 50, 100, and 200  $\mu\text{g}/\text{mL}$ ) with complete medium. MTT solution aliquots at 5 mg/mL in PBS were prepared, followed by culture incubation with this solution at 5% in the culture medium for 4 h in an incubator with a moist atmosphere of 5%  $\text{CO}_2$  at  $37^\circ\text{C}$ . After 4 h, 100  $\mu\text{L}$  of MTT solubilizing solution was added and shaken for 15 min. Finally, the absorbance of the MTT colorimetric assay was measured by Varioskan flash (Thermo Scientific, USA) at a wavelength of 570 nm. The viable quantity of cells was then calculated by the following equation:

$$\text{cell viability (\%)} = (\text{absorbance of sample cells}) / (\text{absorbance of control cells}) \times 100$$

For a cellular uptake study of GQDs and D-GQDs, they were each added and incubated with the KB cell line. The KB cells were cultured at  $37^\circ\text{C}$  in a humidified atmosphere containing 5%  $\text{CO}_2$  in a MEM medium with 10% fetal bovine serum. The cells ( $5 \times 10^4$  cells/mL) were grown as a monolayer, and were harvested by 0.25% trypsin-0.03% EDTA solution. The cells (200  $\mu\text{L}$ ) in their respective media were seeded in an 8-well plate and were preincubated for 24 h before the assay. Both the GQD (0.1 mg/mL) and D-GQD (0.1 mg/mL equivalent to GQDs) formulations were added to 8-well plates and were incubated for 1 h before observation by a confocal laser scanning microscope (CLMS). The wells were washed 5 times with PBS to remove the free particles from the cells. A 4% formaldehyde solution was added to preserve the cells, and the fixed cells were observed by CLMS. The cells were scanned at 530 nm excitation to get PL intensity of GQDs.

**In Vivo Biodistribution and Imaging Study.** Six to seven week-old SKH1 female nude mice (ranges of body weight was 20–23 g) were purchased from Orient Bio INC., (Seoul, Korea) and were maintained under specific pathogen-free conditions. All experiments were approved by institutional guidelines of the Institutional Animal Care and Use Committee (IACUC) of the Catholic University of Korea College of Medicine in accordance with NIH Guidelines. For *in vivo* imaging studies, nude mice were administered with GQDs and pDA-coated GQD nanoparticles (50  $\mu\text{L}$ , 5 mg/kg) respectively through intravenous injection (IV). Mice were then anesthetized with ketamine (87 mg/kg, Virbac Laboratories, France) and xylazine (13

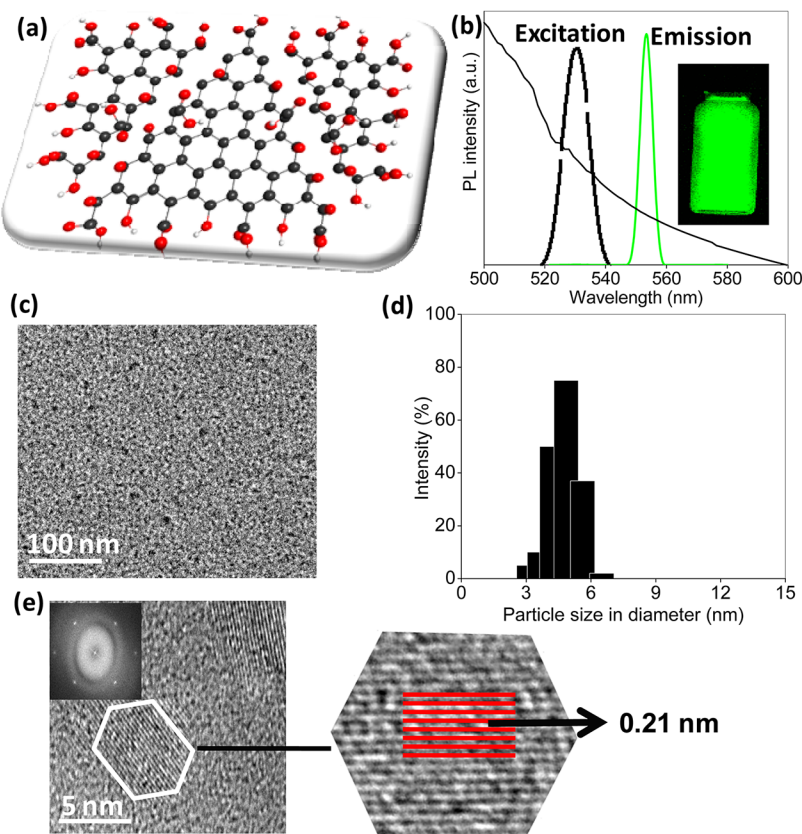


**Figure 1.** Properties of GQDs. (a) Computer simulated structure of GQDs containing carbon (gray), oxygen (red), and hydrogen (white) atoms as carboxylic and hydroxyl functional groups. (b) UV absorbance and photoluminescent excitation and emission spectrum of GQDs. (c) TEM image of GQDs (scale bar indicates 100 nm). (d) Average size distribution of GQDs measured by dynamic light scattering (DLS). (e) HRTEM images of GQDs showing the edge structure of lattice and 2D Fourier transform pattern.

mg/kg, Kepro B.V., Netherland) via intraperitoneal injection, and noninvasive images of GQDs injected mice were taken by a time-domain diffuse optical tomography system. In the Experimental Section, mice were placed on the imaging platform. Images were taken at 4 h post injection. The mice were dissected to isolate the organs and optical ex vivo images were taken to observe biodistribution. The 3D scanning region of interest was selected using a bottom-view charge-coupled device (CCD).<sup>46</sup> All images were taken using the Kodak *in vivo* imaging system (4000MN PRO, Kodak, USA). Exposure time was 30 s, and excitation and emission filter were 530 and 550, respectively.

### 3. RESULTS AND DISCUSSION

**Synthesis and Characterization of Graphene Quantum Dots.** To make monolayered graphene quantum dots, we first performed exfoliation of carbon fiber in a strong acid mixture (cosolvent of sulfuric acid and nitric acid) for 12 h at  $95 \pm 5$  °C. Figure 1 and Scheme S1 in the Supporting Information showed the formation of zigzag shaped graphene quantum dots, containing a number of hydroxyl, carboxyl and keto groups around the edge and surfaces. The PL emission (550 nm) and excitation (530 nm) spectrum of GQDs shows a narrow emission spectra (30–40 nm full width at half-maximum of the spectrum, fwhm) with excellent photoluminescent intensity. From HRTEM, we confirmed that graphene quantum dots have a hexagonal structure and are 4–6 nm in diameter. The hydrodynamic particle size of GQDs was also measured by DLS, shows particle size ranges from 3 to 7 nm in diameters. The GQDs showed negative value in zeta potential measurement due to presence of numerous hydroxyl and carboxyl groups. The water-soluble GQDs dramatically lost

the PL intensities under different conditions (FBS, 10% FBS and 2% NaCl solution) as shown in Scheme S1. The possible reason of unstable PL intensity of GQDs in aqueous solution is due to the charge–charge interactions between protons ( $H^+$ ) generated from  $H_2O$  and negative charged GQDs, resulting in quenching of PL intensity of the GQDs.

**Polydopamine-Coated Graphene Quantum Dots.** To maintain PL intensity of GQDs in water long term, we utilized the self-polymerization of DOPA at pH 8.5. The coating has been performed through two steps; first polydopamine (pDA) was formed from DOPA through vigorous stirring at pH 8.5 at different duration (3, 6, and 12 h) shown in Scheme S2 in the Supporting Information. The polymerization of pDA or repeating unit of DOPA was controlled by controlling polymerization time. The pDA3, pDA6 and pDA12 were characterized by <sup>1</sup>H NMR to estimate degree of polymerization dopamine for 3, 6, and 12 h of reaction, respectively. The results presented in Figure S2 in the Supporting Information show that degree of polymerization is 12, 48, and 97 for pDA3, pDA6 and pDA12, respectively (see Figure S2 in the Supporting Information). DSC analysis of polydopamine-coated GQDs also shows that the molecular weight of D-GQD12 is higher than those of D-GQD3 and D-GQD6. The results obtained from <sup>1</sup>H NMR match with the DSC. Before adding the GQDs, the pH of the pDA containing solvent was controlled to 4.5 to avoid any multilayer coating. The mixture were stirred for 2 h at room temperature as shown in Scheme S3 in the Supporting Information, resulting in the surfaces of GQDs was covered by pDA due to oxidation of catechol

**Table 1.** Size and Zeta Potential of GQDs and pDA-Coated GQDs

formulation	GQDs (mg)	DOPA (mg)	TBS (pH-8.5) mL	reaction period	size (nm)	zeta potential (mV)
GQDs	10	N/A			5 ± 2	-9.26 ± 0.75
DOPA		30	15		N/A	-13.93 ± 1.05
D-GQD3	10	30	15	3	7 ± 2	-19.29 ± 0.22
D-GQD6	10	30	15	6	12 ± 3	-21.33 ± 1.11
D-GQD12	10	30	15	12	21 ± 5	-22.66 ± 0.79

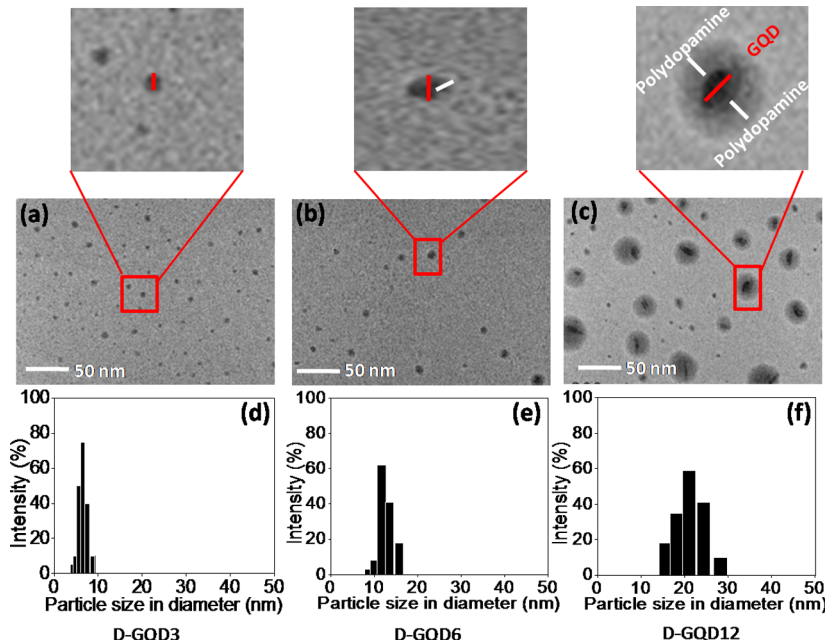


**Figure 2.** Size and morphology of pDA-coated GQDs. TEM images of pDA-coated GQDs (a) D-GQD3, (b) D-GQD6, and (c) D-GQD12 shows the size variation depending on the polymerization time. The magnified TEM images show the pDA layer coated on the GQDs. The average sizes of (d) D-GQD3, (e) D-GQD6, and (f) D-GQD12 are 8, 15, and 24 nm, respectively.

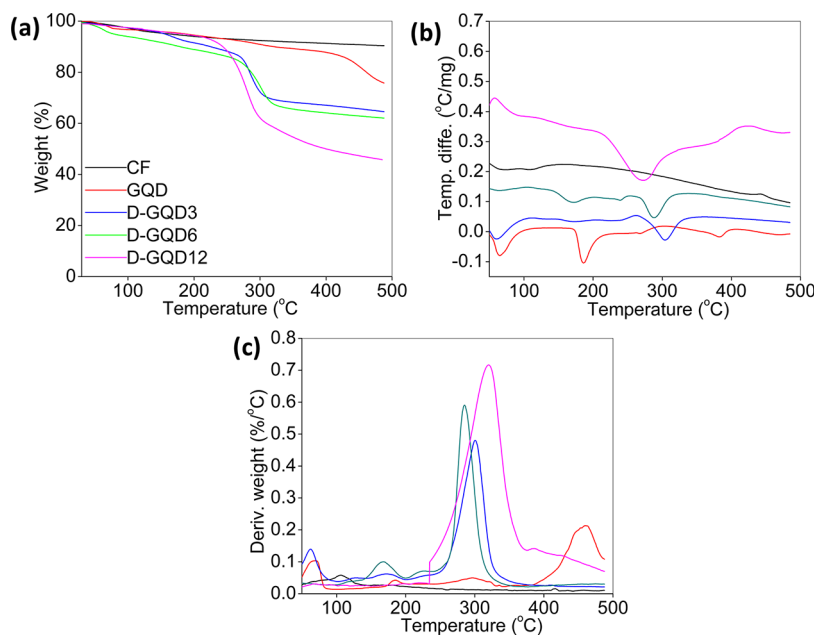


**Figure 3.** Thermal stability of GQDs and pDA-coated GQDs measured by (a) TGA and (b) DTA. (c) Glass transient temperature of GQDs and the coated GQDs. The thermal degradation and thermal profile demonstrated that the surfaces of GQDs have been successfully coated by pDA.

groups.<sup>39</sup> It seems that the catechol of pDA strongly interacts with the surfaces of GQDs through coordination bonding, as shown in Scheme S4 in the Supporting Information. The

successful coating of GQDs was confirmed by FT-IR spectra, as the moieties of DOPA such as catechol and amine groups appeared in FT-IR spectra, as shown in Figure S3. The

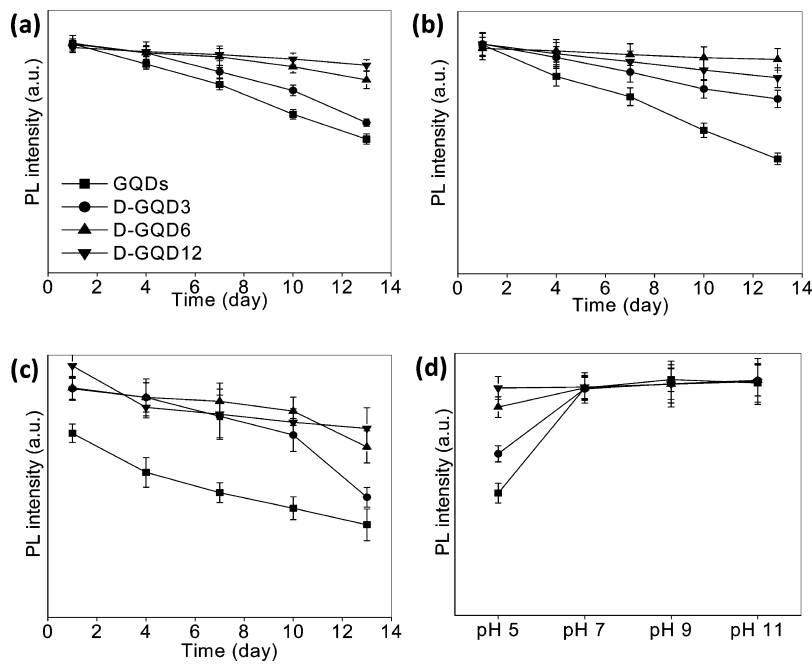


**Figure 4.** In vitro stability of GQDs and pDA-coated GQDs. PL intensities (a) in phosphate buffer saline (PBS), (b) in 10% fetal bovine saline (FBS), (c) in 2% NaCl solution, and (d) in pH buffers for 14 days. Data represent mean  $\pm$  SEM ( $n = 6$ ).

spectrum of pDA-coated GQDs shows the presence of both carboxyl ( $-\text{COOH}$ ,  $\sim 1600 \text{ cm}^{-1}$ ) and amine ( $-\text{NH}$ ,  $\sim 1550$  and  $\sim 1700 \text{ cm}^{-1}$ ) groups as well as hydroxyl ( $-\text{OH}$ ,  $\sim 3400 \text{ cm}^{-1}$ ) functional groups. The as synthesized GQDs and pDA-coated GQDs were further analyzed by XPS. Figure S4 in the Supporting Information shows the C 1s core level XPS survey scanning spectrum of those respective products. The C 1s spectra of GQDs attributable to the C–C, C–O, C=O, and O=C=O whereas pDA-coated GQDs attributable to the C–C, C–N, C–O, C=O, and O=C=O species. The results do not demonstrate any evidence reduction of GQDs due to pDA coating. Figure S5 in the Supporting Information shows the NMR spectrum of DOPA, GQDs, and pDA-coated GQDs. The spectrum confirm the pDA located on the surface or edge of GQDs as the amine ( $-\text{NH}_2$ ) and hydroxyl ( $-\text{OH}$ ) moieties of DOPA confirmed by NMR analysis. The zeta potential showed that each GQDs and DOPA was  $-9.26 \pm 0.75$  and  $-13.93 \pm 1.05$ . After coating with pDA, the zeta potential values of D-GQD3, D-GQD6, and D-GQD12 was slightly increased to  $-19.29 \pm 0.22$ ,  $-21.33 \pm 1.1$ , and  $-22.66 \pm 0.79$  mV, respectively, as shown in Table 1 and Figure S6 in the Supporting Information. From the TEM and DLS observation, the average size of D-GQD12 increased to about 3 times than that of D-GQD3, resulting in a higher polymerization of DOPA with GQDs (Figure 2a–c). The larger particle at D-GQD12 represents the aggregation of two or more nanoparticles. The results demonstrated that the higher polymerization of pDA could link two or more GQDs whereas the shorter polymerization could only coat single GQDs. The DLS data also shows the mean diameter of the D-GQD3, D-GQD6 and D-GQD12 to be 8, 15, and 24 nm, respectively (Figure 2d–f). The thermal properties of pDA-coated GQDs were observed by thermal gravimetric analysis (TGA) and differential thermal analysis (DTA), Figure 3 demonstrated that the weight loss of the pDA-coated GQDs started from  $280^\circ\text{C}$ , whereas carbon fiber was maintained up to  $500^\circ\text{C}$ . D-GQD3, D-GQD6, and D-GQD12 also showed a different weight loss and increased

with increasing amounts of pDA to around 30%. The DTA spectrum of GQDs showed three exothermic peaks, whereas CF did not show any exothermic or endothermic properties. PDA-coated GQDs showed an exothermic peak at around  $300^\circ\text{C}$  (Figure 3b). The glass transient temperatures (TG) of CF, GQD, and pDA-coated GQDs were measured and showed noncoated CF does not have TG up to  $500^\circ\text{C}$ . On the other hand, TG values of GQDs, D-GQD3, D-GQD6 and D-GQD12 are  $460$ ,  $300$ ,  $290$ , and  $320^\circ\text{C}$ , respectively (Figure 3c).

**Stability of Polydopamine-Coated GQDs.** Photoluminescent (PL) stability of GQDs and pDA-coated GQDs were observed in PBS, 10% FBS, pHs (5, 7, 9, and 11) buffers and electrolytes solution (2% NaCl) for 14 days, respectively. Figure 4 shows that the PL intensity of noncoated GQDs in PBS solution rapidly decreased with time, resulting in a 45% reduction of the PL intensity for 14 days of incubation in PBS solution. After coating with pDA, PL intensities of D-GQD3, D-GQD6, and D-GQD12 were maintained stability for 14 days compared with GQDs. Figure 4c also showed a different PL intensity between coated and noncoated GQDs. This dramatic result is likely due to the aggregation or protonation of the surface of GQDs with serum/strong acid, causing quenching of GQDs. PL stability of GQDs and pDA-coated GQDs presented at Figure 4d, measured after 1 h of vortexing. The results demonstrated that the coated GQDs are stable in acidic, neutral and base pH, because the excess proton of acidic buffer could not get in touch of the GQDs due to coated by pDA. Resulted in no PL quenching of GQDs was occurred. However, the free PL intensity GQDs was also stable in pH higher than 7 due to no possibility quenching through charge–charge interaction (negative charged GQDs and proton). From the results, we concluded that the coated pDA on the surface of GQDs provides a barrier to GQDs over the long term. However, dip-coating of GQDs by pDA improves PL stability in aqueous solution due to the covering of the edge and surfaces of GQDs, and therefore quenching did not occur. At the same time, the pDA linked with GQDs through coordination bonding on the

surface of GQDs, which enhances PL stability of GQDs (see Scheme S4 in the Supporting Information). Size stability of GQDs and D-GQDs was also observed for 7 days to observe the changes of diameter of GQDs and D-GQD6 in different media such as PBS, 10% FBS, 2% NaCl solution. The results demonstrate that the GQDs become aggregate as particle size increased. However, no precipitation was observed through naked eyes during those 7 days of observation (see Figure S7 in the Supporting Information).

**In Vitro Cytotoxicity.** The cytotoxicities of GQDs and pDA-coated GQDs were investigated in KB cancer cell lines. Different concentrations (50, 100, 250, and 500  $\mu\text{g}/\text{mL}$ ) of GQDs and the coated GQD were incubated for 24 h and cell viability was measured by MTT colorimetric assay. The results demonstrated that the largest amounts of viable cells are observed in D-GQD12, indicating a direct relationship between cell viability and the amount of pDA. The noncoated GQDs expressed minimal cytotoxicity due to the huge amount of oxygen on the surface and on the edge. However, after coating with biocompatible bioinspired pDA, GQDs do not show any mentionable toxicity in cells, as shown in Figure 5.

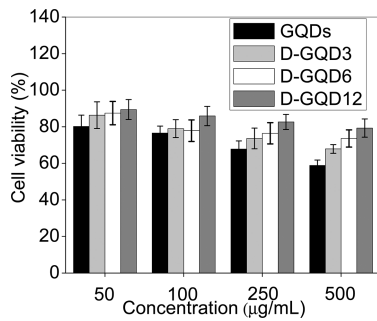


**Figure 5.** In vitro cytotoxicity of GQDs and pDA-coated GQDs. Different concentration of GQDs, D-GQD3, D-GQD6 and D-GQD12 were cocultured with KB cells and were incubated for 24 h to measure cell viability by MTT colorimetric assay. Data represents mean  $\pm$  SEM ( $n = 6$ ).

**In Vitro Cellular Imaging.** Figure 6 shows the cellular uptake profile of GQDs formulations in the KB cells observed by confocal laser scanning microscope after 1 h of incubation with GQDs and pDA-coated GQDs, respectively. The result showed that free GQDs, as well as pDA-coated GQDs are capable of entering into the KB cell line. After 1 h incubation, we could observe strong green color PL intensity from GQDs and pDA-coated GQDs, respectively. The negatively charged GQDs and pDA-coated GQDs were effectively taken up by the cells and observed in the cytoplasm and membrane. The in vitro cell imaging results were well-matched with those of MTT assay. It is assumed that the strong cellular uptake of noncoated GQDs is related with cytotoxicity of GQDs at high concentration. However, the strong optical signal of the coated pDA in the cells may be not related with cytotoxicity, as shown in Figure 6. As further study, we may need to carry out toxicity study with animals in order to determine the long-term effects of such nanoparticles.

**In Vivo Imaging of Polydopamine-Coated GQDs.** To evaluate in vivo biodistribution and bioimaging, pDA-coated GQDs (D-GQD3, D-GQD6 and D-GQD12) and GQDs were dispersed in PBS and were injected into nude mice individually through tail vein. The mice were sacrificed 4 h after i.v. injection, and images were taken by a Kodac Molecular Imaging

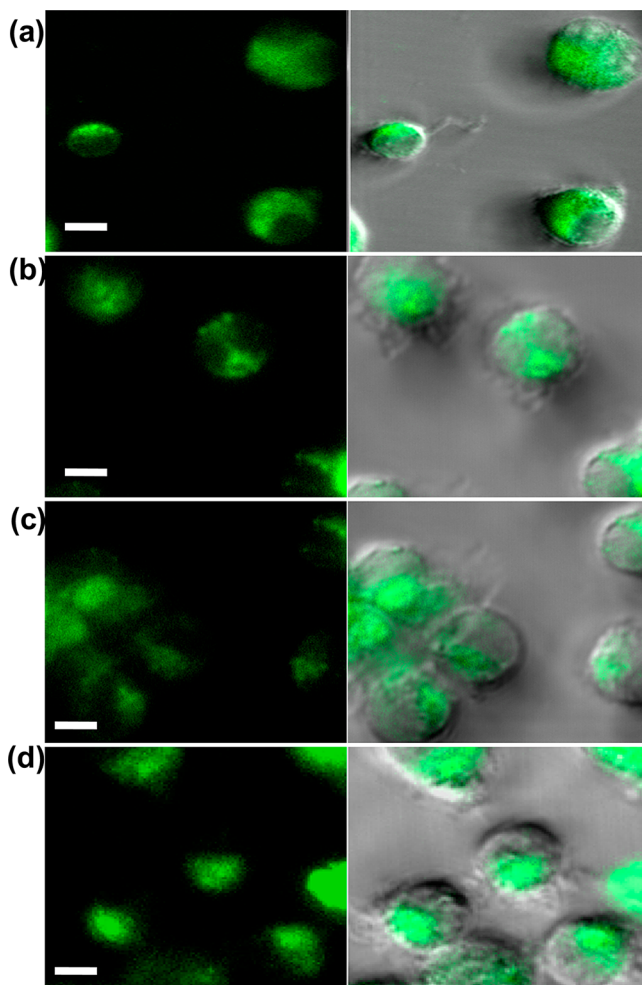


**Figure 6.** In vitro cellular uptake study observed by confocal laser scanning microscope. (a) GQDs, (b) D-GQD3, (c) D-GQD6, and (d) D-GQD12 were cocultured with KB cells and were incubated for 1 h. Scale bar indicates 50  $\mu\text{m}$ .

System (KMIS). The mice were dissected and the organs (lung, kidney, liver, spleen and kidney) were isolated from the mice. The ex vivo images of those isolated organs were then observed by KMIS to distinguish biodistribution, location and accumulation of the administered GQDs and pDA-coated GQDs, respectively. Figure 7 demonstrates the fluorescence images of GQDs and pDA-coated GQDs after i.v. injection in mice. We confirmed that both GQDs and pDA-coated GQDs were distributed into each organ tissue (heart, liver, lung, spleen and kidney) through systemic circulation. The relatively low fluorescence intensity for noncoated GQDs might reflect the rapid renal clearance of GQDs with size in the range of 3–6 nm after 4 h injection. On the other hand, the coated D-GQDs showed stronger fluorescence intensities in each organ than GQDs, except in the lung. In the liver, we found that the fluorescence intensity of mice treated by D-GQD12 is brighter than those of GQDs, D-GQD3, and D-GQD6 injected mice, indicating the presence of D-GQD12 in the liver for a longer period. We assumed two possible ways; one of the reasons is that the PL intensity of D-GQD12 is more stable than those of GQDs, D-GQD3 and D-GQD6. The other is that the excretion rate of D-GQD12 is slower than that of other formulations as the particle size is larger. The different biodistribution profile was also observed due to variation in particle size and

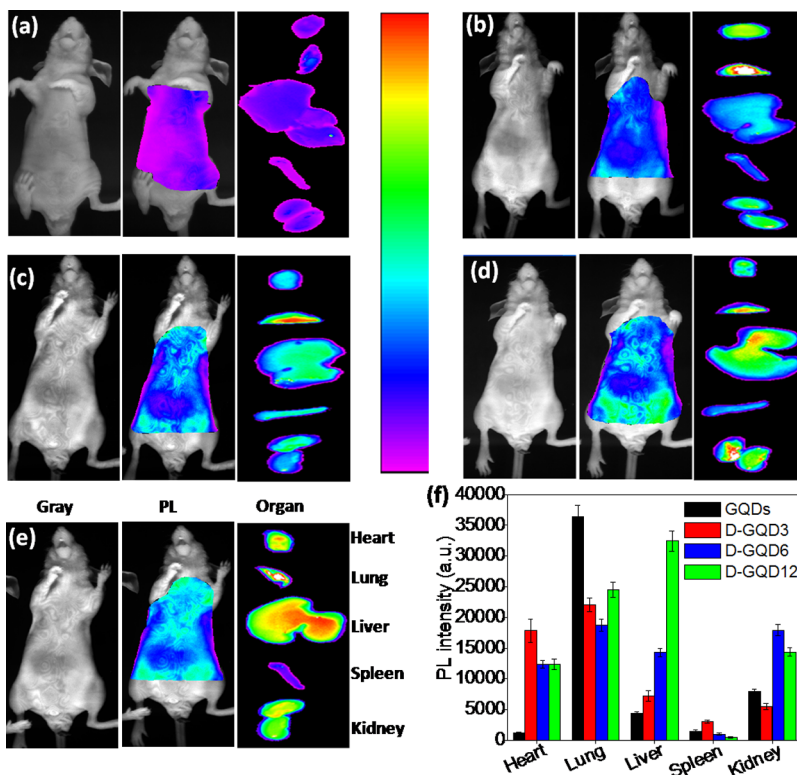


**Figure 7.** In vivo biodistribution and bioimaging of GQDs and the coated GQDs. Optical imaging of nude mice and isolated organs of (a) saline-treated control mice, (b) GQD-treated mice, (c) D-GQD3-treated mice, (d) D-GQD6-treated mice, and (e) D-GQD12-treated mice. (f) PL intensities of each organ tissue after treatment with GQDs and pDA-coated GQDs, respectively.

properties. The in vivo observation and findings from the animal experiments demonstrate that the modification of GQDs by pDA retains PL intensity in the in vivo model. A dramatic biodistribution profile was also observed among the animals treated by different GQDs formulations.

#### 4. CONCLUSIONS

In our study, pDA successfully covered the surfaces of the GQDs by means of catechol chemistry. Our supporting data provided us a broad range of evidence and profiling of surface modification, PL stability and thermal stability. PDA-coated GQDs show better PL stability than noncoated GQDs, maintaining quite stable PL intensities for 14 days. Cell images observed by confocal laser scanning microscope demonstrated that the GQDs and pDA-coated GQDs are promising candidates for single cell imaging. Optical images in nude mice demonstrate visualization to track the location of GQDs found in different organs, such as the liver, spleen and kidney. In vivo biodistribution of the GQDs also show different fluorescence intensities according to the size and coating thickness. Finally, we conclude that the bioinspired catechol chemistry-mediated surface modification of GQDs is a biocompatible and promising method to enhance PL stability for the long-term. The pDA-coated GQDs could be considered as a promising agent for drug and gene delivery. Further studies can be continued based on the surface decoration by different agents such as anticancer drugs and MRI imaging agents or genes, for a novel drug design and delivery.

#### ASSOCIATED CONTENT

##### Supporting Information

Details on synthesis of pDA, scheme for GQDs coating, FT-IR, FT-NMR, and zeta potential are provided. This material is available free of charge via the Internet at <http://pubs.acs.org>.

#### AUTHOR INFORMATION

##### Corresponding Author

\*E-mail: leeyk@ut.ac.kr. Tel: +82-043-841-5224. Fax: +82-043-841-5220.

##### Author Contributions

The manuscript was written through contributions of all authors. All authors have given approval to the final version of the manuscript.

##### Notes

The authors declare no competing financial interest.

#### ACKNOWLEDGMENTS

This research was supported by Basic Science Research Program through the National Research Foundation of Korea (NRF) funded by the Ministry of Education, Science and Technology (2010-0021427).

#### REFERENCES

- (1) Jiang, E.; Gnanaammudhan, M. K.; Zhang, Y. *J. R. Soc. Interface* **2010**, *7*, 3–18.
- (2) Nurunnabi, M.; Cho, K. J.; Choi, J. S.; Huh, K. M.; Lee, Y-k *Biomaterials* **2010**, *31*, 5436–5444.
- (3) Kim, J. S.; Cho, K. J.; Tran, T. H.; Nurunnabi, M.; Moon, T. H.; Hong, S. M.; Lee, Y-k. *J Colloid Interface Sci.* **2011**, *353*, 363–371.

- (4) Shuhendler, A. J.; Prasad, P.; Chan, H.-K. C.; Gordijo, C. R.; Sorourian, B.; Kolios, M.; Yu, K.; O'Brien, P. J.; Rauth, A. M.; Wu, X. Y. *ACS Nano* **2011**, *5*, 1958–1966.
- (5) Cook, J. R.; Frey, W.; Emelianov, S. *ACS Nano* **2013**, *7*, 1272–1280.
- (6) Goh, C.; Li, B. S. *Nano Lett.* **2007**, *7*, 1110–1111.
- (7) Choi, Y.; Hong, S.; Kang, T.; Lee, L. P. *J. Phys. Chem. C* **2009**, *113*, 14587–14590.
- (8) Pauli, J.; Grabolle, M.; Brehm, R.; Spieles, M.; Hamann, F. M.; Wenzel, M.; Hilger, I.; Resch-Genger, U. *Bioconjugate Chem.* **2011**, *22*, 1298–1308.
- (9) Hama, Y.; Urano, Y.; Koyama, Y.; Bernardo, M.; Choyke, P. L.; Kobayashi, H. *Bioconjugate Chem.* **2006**, *17*, 1426–1431.
- (10) Khatun, Z.; Nurunnabi, M.; Choi, K. J.; Lee, Y.-k. *Carbohydr. Polym.* **2012**, *90*, 1461–1468.
- (11) Khatun, Z.; Nurunnabi, M.; Choi, K. J.; Lee, Y.-k. *ACS Appl. Mater. Interfaces* **2012**, *4*, 3880–3887.
- (12) Cassette, E.; Helle, M.; Bezdetnaya, L.; Marchal, F.; Dubertret, B.; Pons, T. *Adv. Drug Delivery Rev.* doi.org/10.1016/j.addr.2012.08.016
- (13) Smith, A. M.; Duan, H.; Mohs, A. M.; Nie, S. *Adv. Drug Delivery Rev.* **2008**, *60*, 1226–1240.
- (14) Bae, P. K.; Kim, K. N.; Lee, S. J.; Chang, H. J.; Lee, C. K.; Park, J. K. *Biomaterials* **2009**, *30*, 836–842.
- (15) Nune, S. K.; Gundu, P.; Thallapally, P. K.; Lin, Y.-Y.; Forrest, M. L.; Berkland, C. J. *Expert Opin Drug Deliv.* **2009**, *6*, 1175–1194.
- (16) Su, Y.; Peng, F.; Jiang, Z.; Zhong, Y.; Lu, Y.; Jiang, X.; Huang, Q.; Fan, C.; Lee, S. T.; He, Y. *Biomaterials* **2011**, *32*, 5855–5862.
- (17) Wang, C.; Gao, X.; Su, X. *Anal. Bioanal. Chem.* **2010**, *397*, 1397–1415.
- (18) Drbohlavova, J.; Adam, V.; Kizek, R.; Hubalek, J. *Int. J. Mol. Sci.* **2009**, *10*, 656–673.
- (19) Alivisatos, A. P.; Gu, W.; Larabell, C. *Annu. Rev. Biomed. Eng.* **2005**, *7*, 55–76.
- (20) Tiwari, D. K.; Jin, T.; Behari, J. *Int. J. Nanomed.* **2011**, *6*, 463–475.
- (21) Wu, W.; Shen, J.; Banerjee, P.; Zhou, S. *Biomaterials* **2010**, *31*, 8371–8381.
- (22) Xie, M.; Luo, K.; Huang, B.-H.; Liu, S.-L.; Hu, J.; Cui, D.; Zhang, Z.-L.; Xiao, G.-F.; Pang, D.-W. *Biomaterials* **2010**, *32*, 8362–8370.
- (23) Gao, J.; Chen, K.; Miao, Z.; Ren, G.; Chen, X.; Gambhir, S. S.; Cheng, Z. *Biomaterials* **2011**, *32*, 2141–2148.
- (24) Li, J.-M.; Zhao, M.-X.; Su, H.; Wang, Y.-Y.; Tan, C.-P.; Ji, L.-N.; Mao, Z.-W. *Biomaterials* **2011**, *32*, 7978–7987.
- (25) Ruan, J.; Song, H.; Qian, Q.; Li, C.; Wang, K.; Bao, C.; Cui, D. *Biomaterials* **2012**, *33*, 7093–7102.
- (26) Chang, J.-C.; Su, H.-L.; Hsu, S.-h. *Biomaterials* **2009**, *29*, 925–936.
- (27) Zheng, X. T.; Than, A.; Ananthanaraya, A.; Kim, D.-H.; Chen, P. *ACS Nano* **2013**, *7*, 6278–6286.
- (28) Štengl, V.; Bakardjieva, S.; Henych, J.; Lang, K.; Kormunda, M. *Carbon* **2013**, DOI: 10.1016/j.carbon.2013.07.031.
- (29) Tang, L.; Ji, R.; Li, X.; Teng, K. S.; Lau, S. P. *J. Mater. Chem. C* **2013**, *1*, 4908–4915.
- (30) Phirouznia, A.; Akbari, N.; Lotfi, S.; Jamshidi-Ghaleh. *Eur. Phys. J. B* **2012**, *85*, 259–265.
- (31) Dong, Y.; Pang, H.; Rem, S.; Chen, C.; Chi, Y.; Yu, T. *Carbon* **2013**, DOI: 10.1016/j.carbon.2013.07.059.
- (32) Zhang, P.; Li, W.; Zhai, X.; Liu, C.; Dai, L.; Liu, W. *Chem. Commun.* **2012**, *48*, 10431–10433.
- (33) Dong, Y.; Pang, J.; Yang, H. B.; Guo, C.; Shao, J.; Chi, Y.; Li, C. M.; Yu, T. *Angew. Chem., Int. Ed.* **2013**, *S2*, 7800–7804.
- (34) Peng, J.; Gao, W.; Gupta, B. K.; Liu, Z.; Romero-Aburto, R.; Ge, L.; Song, L.; Alemany, L. B.; Zhan, X.; Gao, G.; Vithayathil, S. A.; Kaipparettu, B. A.; Marti, A. A.; Hayashi, T.; Zhu, J.-J.; Ajayan, P. M. *Nano Lett.* **2012**, *12*, 844–849.
- (35) Nurunnabi, M.; Khatun, Z.; Reeck, G. R.; Lee, D. Y.; Lee, Y.-k. *Chem. Commun.* **2013**, *49*, 5079–5081.
- (36) Waite, J. h.; Tanzer, M. L. *Science* **1981**, *212*, 1038–1040.
- (37) Joddar, B.; Albayrak, A.; Kang, J.; Nishihara, M.; Abe, H.; Ito, Y. *Acta Biomater.* **2013**, *5*, 6753–6761.
- (38) Xu, L. Q.; Yang, W. J.; Neoh, K.-G.; Kang, E.-T.; Fu, G. D. *Macromolecules* **2010**, *43*, 8336–8339.
- (39) Ku, S. H.; Ryu, J.; Hong, S. K.; Lee, H.; Park, C. B. *Biomaterials* **2010**, *31*, 2535–2541.
- (40) Barras, A.; Lyskawa, J.; Szunerits, S.; Woisel, P.; Boukherroub, R. *Langmuir* **2011**, *27*, 12451–12457.
- (41) Hong, S.; Kim, K. Y.; Wook, H. J.; Park, S. Y.; Lee, K. D.; Lee, D. Y.; Lee, H. *Nanomedicine (Lond.)* **2011**, *6*, 793–801.
- (42) Guo, L.; Liu, Q.; Li, G.; Shi, J.; Liu, J.; Wang, T.; Jiang, G. *Nanoscale* **2012**, *4*, 5864–5867.
- (43) Zhang, Z.; Zhang, J.; Zhang, B.; Tang, J. *Nanoscale* **2013**, *5*, 118–123.
- (44) Nurunnabi, M.; Khatun, Z.; Huh, K. M.; Park, S. Y.; Lee, D. Y.; Cho, K. J.; Lee, Y.-k. *ACS Nano* **2013**, DOI: 10.1021/nn402043c.
- (45) Lee, H.; Dellatore, S. M.; Miller, W. M.; Messersmith, P. B. *Science* **2007**, *318*, 426–430.
- (46) Khatun, Z.; Nurunnabi, M.; Reeck, G. R.; Cho, K. J.; Lee, Y.-k. *Controlled Release* **2013**, *170*, 74–82.